

RESEARCH ARTICLE | FEBRUARY 29 2024

The double surge wave generated by a supercritical flow entering upstream of a pre-existing current

Andrea Defina  



Physics of Fluids 36, 027144 (2024)

<https://doi.org/10.1063/5.0193292>



Physics of Fluids

Special Topic:

Kitchen Flows 2024

Guest Editors: Gerald G. Fuller, Maciej Lisicki, Arnold J.T.M. Mathijssen, Endre Joachim Mossige, Rossana Pesquino, Vivek Nagendra Prakash, Laurence Ramos

[Submit Today!](#)

The double surge wave generated by a supercritical flow entering upstream of a pre-existing current

Cite as: Phys. Fluids **36**, 027144 (2024); doi: [10.1063/5.0193292](https://doi.org/10.1063/5.0193292)

Submitted: 21 December 2023 · Accepted: 31 January 2024 ·

Published Online: 29 February 2024



View Online



Export Citation



CrossMark

Andrea Defina^{a)}

AFFILIATIONS

Department of Civil, Environmental and Architectural Engineering, University of Padova, 35131 Padova, Italy

^{a)} Author to whom correspondence should be addressed: andrea.defina@unipd.it

ABSTRACT

The paper discusses a particular phenomenon that develops in an open channel flow when a supercritical current enters from upstream a pre-existing current. In this case, a system of two surge waves, which propagate downstream while distancing each other, develops; the two surges can be either positive or negative, as well as shock or diffuse waves, and arrange into four different configurations. A model of the double surge wave system that allows to estimate the waves characteristics such as the height and the speed of the wave fronts, is described and discussed, and a criterion to predict the wave configuration is proposed. The model is then tested against the results of lab experiments that confirmed its reliability. Some numerical simulations are also performed to describe and further discuss the double surge wave system that develops under different conditions of practical interest.

© 2024 Author(s). All article content, except where otherwise noted, is licensed under a Creative Commons Attribution (CC BY) license (<https://creativecommons.org/licenses/by/4.0/>). <https://doi.org/10.1063/5.0193292>

I. INTRODUCTION

This investigation originates from a recent work by Lazzarin *et al.*⁹ who studied some unresolved aspects of the free orifice-flow under vertical sluice gates by performing both laboratory and numerical experiments. In particular, they performed a numerical study to explore the transition from non-orifice to orifice flow conditions by starting from a steady non-orifice flow and by gradually increasing the flow rate, and hence the flow depth, until the free surface lightly touches the lip of the gate. As soon as this condition occurs, free out-flow suddenly establishes generating a positive shock wave that migrates upstream of the gate and a system of two waves, i.e., a faster positive shock wave followed by a slower negative shock wave, both traveling downstream of the gate. On one hand, negative waves are typically smooth diffuse rather than shock waves and, on the other hand, two different waves are generated downstream of the gate with one single operation; both these unexpected occurrences are worthy of being analyzed in-depth.

Looking into the literature, I could find that the issue, in its general form, i.e., the double surge system that develops when a supercritical flow enters from upstream a pre-existing current, has been studied in the past by Montuori¹¹ and by Montuori and Greco.¹² However, although it is not so uncommon to come across problems where this phenomenon develops, the problem and its solution are not widely

known. Practical applications include, e.g., the surge waves generated in an open channel receiving tailwater downstream of a dam or a hydropower plant.

The present work aims to recall the issue to improve the theoretical solution (by including the case when the upstream wave remains stuck to the most upstream cross section where it has been generated and by proposing a new criterium to distinguish between the possible double surge waves configurations) and to provide the necessary additional experimental and numerical evidence. It is important to stress that the aim of the present work is to draw a simple but effective framework within which to discuss, with an acceptable accuracy, the generation and the main characteristics of a double surge wave system.

Section II describes the theoretical model and the domain of existence of the different double surge configurations; the results of laboratory experiments and numerical simulations are given and discussed in Sec. III; Sec. IV provides some conclusions.

II. A THEORETICAL MODEL FOR THE DOUBLE SURGE WAVE SYSTEM

Starting from a given, nearly uniform, flow with velocity U_0 and depth Y_0 , the flow at the most upstream cross section is suddenly changed by simultaneously imposing a flow velocity U_1 and a depth Y_1

such that $F_1 = U_1/\sqrt{gY_1} > 1$; these conditions are then maintained constant in time. This single operation generates two surge waves that travel downstream at different speeds so that they get further and further apart from each other; in addition, the flow depth and velocity between the two surges remain nearly constant both in time and in space. The four possible wave configurations, identified by Montuori,¹¹ are given in Fig. 1.

Interestingly, the upstream wave of the configurations A and C is a downstream moving the negative shock wave, which is, in fact, rather unusual because negative waves typically expand to form smooth diffuse waves; also, the upstream wave of the configurations B and D is an unusual positive diffuse wave rather than a shock wave that is largely more frequent.

A. Why two waves rather than one?

Let us consider one surge moving downstream at speed a against a flow of velocity U_0 and depth Y_0 . Let U_1 and Y_1 be the flow velocity and depth just upstream of the surge, respectively. In the frame reference of the shock wave front, momentum and mass balance equations provide two relationships between the three unknowns, U_1 , Y_1 , and a ;¹⁶ therefore, only one, among these variables, can be prescribed. If, as in the case of an upstream supercritical flow, both U_1 and Y_1 are given, two waves develop.

B. The model equations

The theoretical model is based on momentum and mass balance equations in the frame reference of the two waves, as approached by Montuori.¹¹ The model uses a wide rectangular channel, so that equations can be written per unit width, and considers any of the flow configurations of Fig. 1 without distinguishing positive from negative, as well as, shock from diffuse waves; in addition, bed slope and bed friction are both assumed negligibly small.

In the frame reference of the upstream surge, mass and momentum balance equations across the surge can be written as

$$(U_1 - a_u)Y_1 = (U_2 - a_u)Y_2, \quad (1)$$

$$\frac{Y_1^2}{2} + (U_1 - a_u)^2 \frac{Y_1}{g} = \frac{Y_2^2}{2} + (U_2 - a_u)^2 \frac{Y_2}{g}. \quad (2)$$

In the above equations, Y_1 and U_1 (or one of the two, and a combination thereof) are given, and the unknowns are the flow depth Y_2 , the velocity U_2 and the speed of the surge, a_u .

Similarly, in the frame reference of the downstream surge, the mass and momentum balance equations across the surge can be written as

$$(U_2 - a_d)Y_2 = (U_0 - a_d)Y_0, \quad (3)$$

$$\frac{Y_2^2}{2} + (U_2 - a_d)^2 \frac{Y_2}{g} = \frac{Y_0^2}{2} + (U_0 - a_d)^2 \frac{Y_0}{g}. \quad (4)$$

In Eqs. (3) and (4), Y_0 and U_0 are given, whereas the surge speed, a_d , and Y_2 and U_2 are unknown.

On the whole, we have a set of four equations to solve for the four unknowns that are the flow depth Y_2 , the velocity U_2 , and the speed of the two surges, a_u and a_d . In particular, combining Eqs. (1) and (2) to eliminate U_2 yields

$$a_u = U_1 - \sqrt{gY_2} \sqrt{\frac{Y_1 + Y_2}{2Y_1}}. \quad (5)$$

Similarly, combining Eqs. (3) and (4) to eliminate U_2 yields

$$a_d = U_0 + \sqrt{gY_2} \sqrt{\frac{Y_0 + Y_2}{2Y_0}}. \quad (6)$$

An iterative procedure to solve the above system of four equations is given in Appendix A.

It is worth pointing that the momentum balance equation is not well suited to describe either negative or positive diffuse waves, which instead required an energy conserving approach such as the method of characteristics. However, with the latter approach, the overall solution becomes formally more complex with negligibly minor improvements. In fact, if diffuse wave fronts are not too height, the momentum balance equation can be applied to determine approximately the propagation of a diffuse surge.¹⁶ This is also confirmed by the comparison, discussed in Sec. II, between the predictions of the theoretical model and the results of a numerical model that solves the Shallow Water Equations (SWEs).

The method of characteristics also provides an accurate description of the diffuse front shape. Here, a sufficiently accurate solution is found by estimating the speed of the head and the toe of the diffuse wave and hence their position at each instant of time; in addition, if the surge wave is not too height, the water depth between the two wave ends can be approximated as linearly varying. In particular, for the upstream surge of configurations B and D, the speed of the head and the toe is, respectively, $a_{u1} = U_1 - \sqrt{gY_1}$ and $a_{u2} = U_2 - \sqrt{gY_2}$,

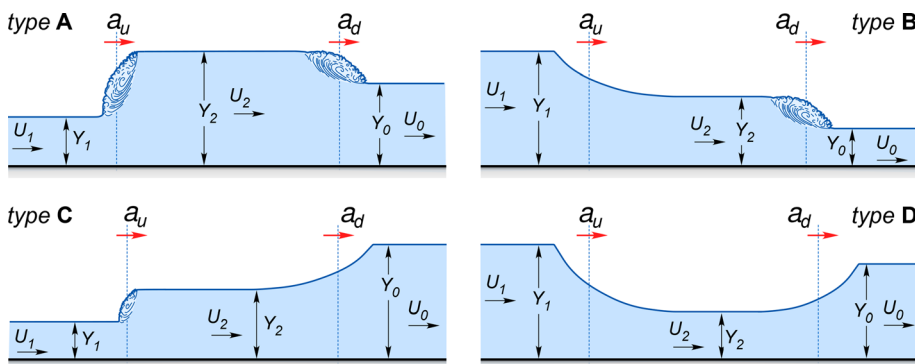


FIG. 1. Schematic of the four possible double surge systems generated by a supercritical flow suddenly entering upstream of a preexisting current; a_u and a_d are the speed of the upstream and the downstream surge waves, respectively; note that, in type A, Y_1 can be greater than Y_0 and, in type D, Y_1 can be lower than Y_0 .

whereas, for the downstream surge of configurations C and D, the speed of the head and the toe are, respectively, $a_{d2} = U_0 + \sqrt{gY_0}$ and $a_{d1} = U_2 + \sqrt{gY_2}$.

C. Domain of existence of the four flow configurations

To identify the domain of existence of the four different flow configurations, we consider the Froude number, $\tilde{F}_1 = \tilde{U}_1 / \sqrt{gY_1}$ that the incoming supercritical current should possess, for a given water depth Y_1 , for one single surge to develop in the channel; we then compare \tilde{F}_1 with the actual Froude number F_1 , and on the basis of this comparison, we can predict which of the four configurations of Fig. 1 will develop in the channel.

Let us consider one surge moving downstream at velocity, a , against a flow of velocity U_0 and depth Y_0 ; let \tilde{U}_1 and Y_1 be the flow velocity and depth just upstream of the surge, respectively. In the frame reference of the shock wave front, the mass and momentum balance equations are given as

$$(\tilde{U}_1 - a)Y_1 = (U_0 - a)Y_0, \quad (7)$$

$$\frac{Y_1^2}{2} + (\tilde{U}_1 - a)^2 \frac{Y_1}{g} = \frac{Y_0^2}{2} + (U_0 - a)^2 \frac{Y_0}{g}. \quad (8)$$

Combining the above two equations to eliminate \tilde{U}_1 yields

$$a = U_0 \pm \sqrt{gY_0} \sqrt{\frac{1}{2} \left(\frac{Y_1^2}{Y_0^2} + \frac{Y_1}{Y_0} \right)}. \quad (9)$$

Equation (7), with the surge velocity, a , given by Eq. (9) yields

$$\tilde{F}_1 \sqrt{\frac{Y_1}{Y_0}} = F_0 \pm \left(1 - \frac{Y_0}{Y_1} \right) \sqrt{\frac{1}{2} \left(\frac{Y_1^2}{Y_0^2} + \frac{Y_1}{Y_0} \right)}. \quad (10)$$

By posing $\eta = Y_0/Y_1$ and $\Delta = (1 - \eta)\sqrt{(1/\eta + 1)/2}$, the above equation can be rewritten as

$$\tilde{F}_1 = F_0 \sqrt{\eta} \pm \Delta. \quad (11)$$

We finally compare \tilde{F}_1 with the actual Froude number ($F_1 \leq \tilde{F}_1$); given the two options provided by the plus or minus symbol in Eq. (11), we have four different conditions, each related to a specific flow configuration among those of Fig. 1; in particular,

$$\begin{aligned} \text{type A} & \text{ if } F_1 > F_0 \sqrt{\eta} + \Delta \text{ and } F_1 > F_0 \sqrt{\eta} - \Delta, \\ \text{type B} & \text{ if } F_1 < F_0 \sqrt{\eta} + \Delta \text{ and } F_1 > F_0 \sqrt{\eta} - \Delta, \\ \text{type C} & \text{ if } F_1 > F_0 \sqrt{\eta} + \Delta \text{ and } F_1 < F_0 \sqrt{\eta} - \Delta, \\ \text{type D} & \text{ if } F_1 < F_0 \sqrt{\eta} + \Delta \text{ and } F_1 < F_0 \sqrt{\eta} - \Delta. \end{aligned} \quad (12)$$

It is interesting to observe that the first condition, i.e., $F_1 \leq F_0 \sqrt{\eta} + \Delta$, controls the upstream wave that can be either a negative shock wave (when $F_1 > F_0 \sqrt{\eta} + \Delta$) or a positive diffuse wave (when $F_1 < F_0 \sqrt{\eta} + \Delta$), whereas the second condition, i.e., $F_1 \leq F_0 \sqrt{\eta} - \Delta$, controls the downstream wave (which is a positive shock wave when $F_1 > F_0 \sqrt{\eta} - \Delta$ and a negative diffuse wave when $F_1 < F_0 \sqrt{\eta} - \Delta$). It is also interesting to observe that the condition $F_1 > 1$ implies (i) $\Delta > 0$ or, equivalently, $\eta < 1$, for the type B configuration, and (ii) $\Delta < 0$, hence $\eta > 1$, for the type C configuration.

In addition, for the surge system of type D to develop, the undisturbed flow must be supercritical, i.e., $F_0 > 1$ (see Appendix C). The domain of existence of the four flow configurations is drawn in Fig. 2.

Differently from the criterion proposed by Montuori,¹¹ the present one is based only on the undisturbed (F_0 , Y_0) and boundary (F_1 , Y_1) conditions and does not explicitly include the intermediate flow (Y_2 , F_2) that depends on the model solution. In addition, here below, we distinguish the case when both surges travel downstream at different speeds, from the case when the upstream surge remains stuck to the most upstream cross section where boundary conditions are prescribed.

When the upstream surge is a diffuse wave, as for the flow configurations B and D, necessarily, both surges travel downstream; in fact, the front of the upstream surge has a speed $a_{u1} = U_1 - \sqrt{gY_1} > 0$ given that $F_1 > 1$. On the contrary, for the flow configurations A and C, the upstream surge is a shock wave and it moves downstream if, and only if, $a_u > 0$.

To represent this constraint on the $(F_0 \sqrt{\eta}/F_1) - (\Delta/F_1)$ diagram of Fig. 2, we start finding the conditions such that $a_u = 0$. We set the velocity U_2 solved from Eq. (1) equal to the velocity U_2 solved from Eq. (3)

$$(U_1 - a_u) \frac{Y_1}{Y_2} + a_u = (U_0 - a_d) \frac{Y_0}{Y_2} + a_d.$$

The above equation, with a_d given by Eq. (6) and with $a_u = 0$, yields

$$U_1^* \frac{Y_1}{Y_2} = U_0 + \sqrt{gY_2} \left(1 - \frac{Y_0}{Y_2} \right) \sqrt{\frac{Y_0 + Y_2}{2Y_0}}, \quad (13)$$

with U_1^* being the upstream flow velocity such that $a_u = 0$. Equation (5), with $a_u = 0$, is solved for $U_1 = U_1^*$ to yield

$$U_1^* = \sqrt{gY_2} \sqrt{\frac{Y_1 + Y_2}{2Y_1}}. \quad (14)$$

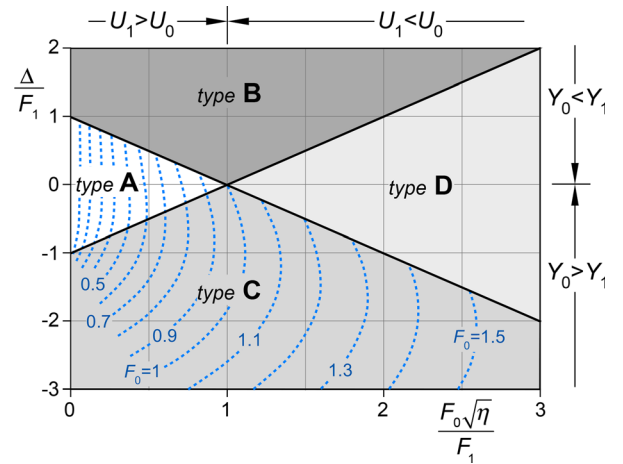


FIG. 2. The domain of the existence of the four possible flow configurations A, B, C, and D. For types A and C, the iso- F_0 dashed curves (F_0 spacing is 0.1) separate the case when both surges travel downstream (left of the curve corresponding to the undisturbed Froude number, F_0) from the case when the upstream surge remains stuck to the most upstream cross section where boundary conditions are prescribed (right of the iso- F_0 curve).

Given the undisturbed flow, U_0 and Y_0 , the solution of the system of Eqs. (13) and (14), for any given flow depth Y_1 , allows us to evaluate what the minimum upstream velocity U_1^* such that both surges travel downstream. Let $\theta = Y_2/Y_1$; with $\eta = Y_0/Y_1$, the system of Eqs. (13) and (14) is rewritten as

$$\sqrt{\eta(\theta + 1)} = F_0 \eta \sqrt{2\theta} + (\theta - \eta) \sqrt{\eta + \theta}, \quad (15)$$

$$F_1^* = \sqrt{\theta} \sqrt{\frac{1}{2}(1 + \theta)}. \quad (16)$$

For given F_0 and η , the Froude number, F_1^* , can be computed from Eq. (16) after solving Eq. (15) for θ . The threshold curves Δ/F_1^* as a function of $F_0 \sqrt{\eta}/F_1^*$, for some values of F_0 , are plotted in Fig. 2 (dashed lines). Only if $F_1 > F_1^*$, the double surge system of type A or C can develop with both waves traveling downstream; on the contrary, if $1 < F_1 < F_1^*$, the upstream surge remains stuck to the most upstream cross section where it has been generated and the downstream wave can be either a positive shock wave or a negative diffuse wave according to a criterion different from that given by Eq. (12), as shown in Sec. II D. Interestingly, this constraint is very tight when the Froude number of the undisturbed flow, F_0 , is relatively small.

D. The case when the upstream wave is stopped

The case when $1 < F_1 < F_1^*$, not considered by Montuori, deserves to be examined and discussed. When $F_1 < F_1^*$, the theoretical model predicts $a_u < 0$, which is not an acceptable solution; in fact, in this case, the upstream wave is stopped by the incoming supercritical current (an example is discussed in Sec. III B 2) or by the device that generates the upstream supercritical current (an example is discussed in Sec. III A 2, in which a vertical sluice gate is suitably operated to generate submerged flow conditions so that the upstream surge is supported by the downstream face of the gate). Accordingly, while Eq. (2) requires an additional source term, i.e., an additional external force, to correctly express the momentum flux equilibrium, Eq. (1), with $a_u = 0$, still holds, and hence $U_2 = U_1 Y_1/Y_2$; with this, Eqs. (3) and (4) can be rewritten as

$$\left(\frac{U_1 Y_1}{Y_2} - a_d \right) Y_2 = (U_0 - a_d) Y_0, \quad (17)$$

$$\frac{Y_2^2}{2} + \left(\frac{U_1 Y_1}{Y_2} - a_d \right)^2 \frac{Y_2}{g} = \frac{Y_0^2}{2} + (U_0 - a_d)^2 \frac{Y_0}{g}. \quad (18)$$

Combining the above two equations to eliminate a_d yields

$$Y_2 = Y_0 - \frac{U_0 Y_2 - U_1 Y_1}{\sqrt{g Y_2}} \sqrt{\frac{2 Y_0}{Y_2 + Y_0}}. \quad (19)$$

Once Eq. (19) is solved for Y_2 (an iterative procedure to compute Y_2 is suggested in Appendix A), the flow velocity and the downstream wave speed are given as

$$U_2 = U_1 \frac{Y_1}{Y_2}, \quad a_d = \frac{U_1 Y_1 - U_0 Y_0}{Y_2 - Y_0}. \quad (20)$$

Figure 3 shows the two possible flow configurations. The wave speed a_d in Eq. (20) must be greater than zero; therefore, when $q_1 = U_1 Y_1 = U_2 Y_2 > U_0 Y_0$, it must be $Y_2 > Y_0$ and the configuration Aw develops [Fig. 3(a)]. On the contrary, when $q_1 = U_1 Y_1 = U_2 Y_2 < U_0 Y_0$, it must be $Y_2 < Y_0$ and the wave configuration Cw

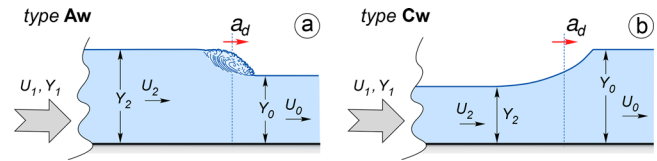


FIG. 3. The case when the upstream wave is stopped. (a) Downstream positive wave developing when $U_1 Y_1 > U_0 Y_0$ (wave configuration Aw) and (b) downstream negative wave developing when $U_1 Y_1 < U_0 Y_0$ (wave configuration Cw). The flow field upstream of the reach where the flow depth and velocity are Y_2 and U_2 is not shown because it depends on the mechanism that causes the upstream wave to stop.

develops [Fig. 3(b)]. Interestingly, when $U_0 = 0$, the flow configuration Cw cannot develop.

Overall, the model given by Eqs. (1)–(4) can be used only if both the upstream and downstream waves are predicted to travel downstream; otherwise, the intermediate flow (i.e., Y_2 and U_2) as well as the speed of the downstream wave can be estimated with Eqs. (19) and (20).

III. EXPERIMENTAL AND NUMERICAL INVESTIGATIONS WITH DISCUSSION

A. Experimental investigations

Before introducing the present experimental study, the data available in the literature, i.e., the data of Montuori and Greco,¹² are reported and discussed both for the sake of completeness and to justify some of the choices made in the design of present experiments.

Both Montuori and Greco¹² and present experiments use a vertical sluice gate to generate the upstream supercritical current and hence the double surge system. When comparing the model predictions to the experimental results, some aspects of this experimental procedure must be kept in mind; in fact, the theory assumes that the supercritical flow enters instantaneously upstream of a pre-existing current, whereas in the experiments, the transient phase, generated by the gate operation, is rapid but not instantaneous and it affects the flow close to the gate.

1. Available experimental data

Montuori and Greco¹² performed a series of experiments to study the double surge generated by a supercritical flow entering from upstream a pre-existing current (see Table I). They used a horizontal flume 18 m long and 0.77 m wide; a downstream gate was operated, if needed, to control the flow depth, Y_0 , whereas a sluice gate, placed approximately halfway, was used to produce the upstream supercritical flow with depth Y_1 and velocity U_1 . Starting from different initial flows, they generated the upstream supercritical flow by suitably lifting or lowering the vertical sluice gate; in particular, in Runs 1–4, starting from free outflow conditions, the gate was quickly lowered; in Runs 5–19, starting from nearly uniform flow, with the gate lip well above the free-surface, the gate was quickly lowered to generate free outflow conditions; in Runs 20–22, starting from free outflow conditions, the gate was quickly lifted maintaining a free outflow; finally, in Runs 27 and 28, starting from submerged flow conditions, the gate was quickly lifted to generate a free outflow. Measurements were taken with point gauges by matching as well as possible the quasi-steady flow depth during the unsteady flow; for this reason, the flow depth in the intermediate region, Y_2 , as well as the flow depth just upstream of the

TABLE I. Summary of Montuori and Greco¹² experimental data; Y_0 and q_0 are the undisturbed flow depth and the flow rate per unit width, Y_A and Y_B are the measured flow depth just upstream of the gate, respectively, before and after the gate is operated, w_0 and w_1 are the gate openings just before and after the gate is operated, respectively, Y_1 is the flow depth of the upstream supercritical current generated by the sluice gate, Y_2 is the intermediate flow depth, and a_u and a_d are the velocity of the upstream and downstream surges, respectively.

RUN	Type	q_0 (m ² s ⁻¹)	Y_0 (m)	w_0 (m)	Y_A (m)	Y_B (m)	w_1 (m)	Y_1 (m)	Y_2 (m)	a_u (m s ⁻¹)	a_d (m s ⁻¹)
1	C	0.130	0.062	0.10	0.290	0.320	0.02	0.012	0.040	1.50	...
2	C	0.130	0.062	0.10	0.290	0.305	0.04	0.025	0.045	1.42	...
3	C	0.182	0.091	0.15	0.280	0.370	0.02	0.012	0.060	1.40	...
4	C	0.182	0.093	0.15	0.280	0.330	0.04	0.025	0.065	1.45	...
5	C	0.130	0.157	0.260	0.02	0.013	0.095	0.04	...
6	C	0.130	0.157	0.245	0.04	0.025	0.115	0.15	...
7	C	0.130	0.157	0.190	0.10	0.062	0.145	0.07	...
8	C	0.156	0.174	0.300	0.02	0.013	0.105	0.05	...
9	C	0.156	0.174	0.285	0.04	0.025	0.125	0.17	...
10	C	0.156	0.174	0.230	0.10	0.062	0.155	0.12	...
11	C	0.182	0.189	0.330	0.02	0.013	0.110	0.04	...
12	C	0.182	0.189	0.310	0.04	0.025	0.135	0.18	...
13	C	0.182	0.189	0.255	0.10	0.061	0.165	0.17	...
14	C	0.208	0.200	0.355	0.02	0.013	0.115	0.06	...
15	C	0.208	0.200	0.335	0.04	0.025	0.145	0.21	...
16	C	0.208	0.200	0.285	0.10	0.060	0.175	0.19	...
17	C	0.234	0.210	0.370	0.02	0.012	0.125	0.12	...
18	C	0.234	0.210	0.350	0.04	0.025	0.150	0.30	...
19	C	0.234	0.210	0.310	0.10	0.060	0.175	0.27	...
20	B	0.040	0.012	0.019	0.570	0.430	0.19	0.116	0.025	...	4.00
21	B	0.019	0.006	0.01	0.570	0.435	0.19	0.115	0.020	...	3.80
22	B	0.066	0.024	0.038	0.459	0.310	0.19	0.115	0.035	...	3.60
27	A	0.011	0.100	0.008	0.329	0.220	0.0935	0.057	0.165	0.10	1.45
28	A	0.016	0.122	0.01	0.503	0.410	0.0935	0.061	0.230	0.17	1.96

sluice gate detected after the gate is operated, Y_B , have an accuracy of only 5 mm. The images of a fixed camera with a frame rate of approximately 3 fps were also used to inspect the measurements. The speed of the surges was estimated by measuring the time they spent to travel preset distances.

The speed of the diffuse wave fronts was not measured due to the difficulty of identifying a certain average speed of the front in the experiments. Also, velocity U_1 was not measured, but estimated using the standard equation for the flow rate per unit width, q_1 , issuing under a vertical sluice gate^{8,13}

$$U_1 = q_1 / (c_c w_1) \quad \text{with} \quad q_1 = c_{q1} w_1 \sqrt{2gY_B} \quad \text{and} \quad c_{q1} = \frac{c_c}{\sqrt{1 + \frac{w_1 c_c}{Y_B}}}, \quad (21)$$

where Y_B and w_1 are the measured flow depth just upstream of the gate and the gate opening, after the gate was operated, and c_c is the contraction coefficient they assumed to be $c_c = 0.62$. To reduce experimental uncertainties, all runs were repeated several times.

In all experiments, the conditions $F_1 > 1$ and $F_1 > F_1^*$ were fulfilled, and the detected configuration types match the present criterion. However, in Runs 27 and 28, initial conditions (subscript "0")

downstream and close to the gate do not match the model assumption of the uniform vertical profile of the streamwise velocity, implicitly assumed in Eqs. (3) and (4), as shared by Montuori;¹¹ therefore, these experiments do not strictly prove the accuracy of the model to describe the surge configuration of type A. For the same reason, the Froude number F_0 cannot be defined in this case. Finally, no experiments producing the surge wave configuration of type D were performed.

We compare these experimental data with the prediction of the present theoretical model; the results of this comparison are summarized in Fig. 4.

The water depth Y_2 of the intermediate flow [Fig. 4(a)] is well predicted by the model when the wave configuration C is forced to form (Runs 1–19); on the contrary, the theoretical model overpredicts Y_2 by approximately 30% for configuration B.

Figure 4(b) compares the measured to the computed speed of shock waves scaled by $c_0 = \sqrt{gY_0}$. The speed of the downstream wave for configuration B is well predicted by the model; the same goes for the case of configuration C when the double surge is generated starting from free outflow conditions. On the contrary, when the gate is quickly lowered starting from nearly uniform flow, the speed of the upstream wave front is inaccurately predicted by the model; this is possibly because the wave speed is actually very slow and a small absolute error appears as a large relative error.

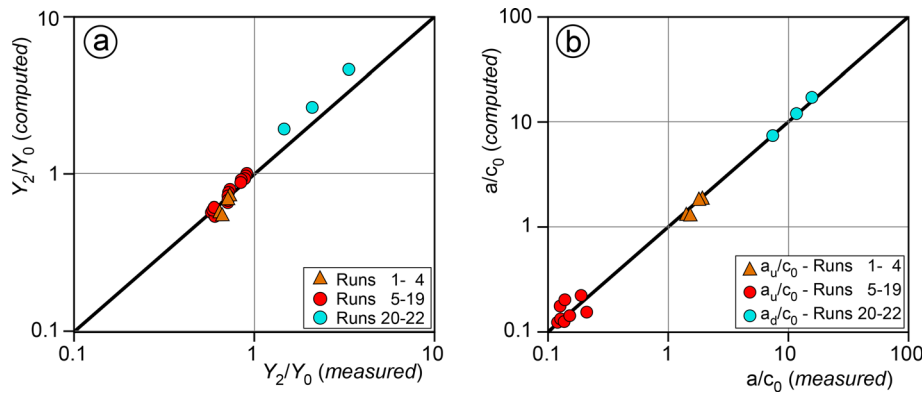


FIG. 4. Comparison between experimental data by Montuori and Greco² and the prediction of the present theoretical model; (a) measured vs computed relative depth of the intermediate flow, Y_2/Y_0 ; (b) measured vs computed relative wave speed a/c_0 .

2. Present experimental investigation

The experiments use a 6 m long, 0.3 m wide, and 0.5 m high tilting flume with Plexiglas walls; water is recirculated via a constant head tank that maintains steady flow conditions, and a downstream weir can be adjusted to control the flow depth, when subcritical.¹⁸ A vertical sluice gate, located approximately halfway the flume, and allowed to slide in grooves that are set in the walls of the flume, is operated to generate the double surge waves (see Fig. 5). A magnetic flowmeter measures the flow rate (accuracy of about 0.2%) and four ultrasonic water level sensors (accuracy of about 0.13 mm, acquisition frequency = 100 Hz), suitably distributed along the flume, records the flow depth both upstream and downstream of the sluice gate. A fixed high speed camera, with a frame rate of 30 fps, records a side view of the unsteady phenomenon; the recorded videos are used to check if any problem occurred during the short transient after the sudden gate operation to when waves have passed the most downstream ultrasonic sensor.

A first series of experiments (SET 1) includes the same experiments performed by Montuori and Greco,¹² in which the different wave configurations are generated only by operating the vertical sluice gate; in particular, we follow the experimental procedures listed below.

Procedure 1. Starting from the free outflow conditions with the gate opening w_0 , the gate is suddenly pushed downward and suitable supports, of length w_1 , inserted in the grooves, arrest the gate at the wanted opening $w_1 < w_0$. This procedure allows generating a wave configuration of type C.

Procedure 2. Starting from the uniform flow conditions with the supports of length w_1 inserted in the grooves, the gate is suddenly lowered to penetrate the flow and generate the free outflow conditions with the gate opening w_1 . This procedure allows generating a wave configuration of type C.

Procedure 3. The gate is set on place with opening w_1 , and a second, sharp crested panel is placed very close upstream of the sluice gate creating a temporary opening of height $w_0 < w_1$; as soon as the steady free outflow conditions are achieved, the second panel is suddenly removed determining free outflow under the fixed gate with opening w_1 . This procedure, which simulates a sudden gate lifting, allows generating a wave configuration of type B.

Procedure 4. The gate is set on place with opening w_1 , and a second panel is placed immediately upstream of the gate to temporarily close the opening; the flume downstream of the gate is filled with still water to the depth Y_0 , whereas the upstream reach of the flume is filled with still water to the depth $Y_A > Y_0$. Starting from these conditions, the second panel is suddenly removed to generate free outflow and the wave configuration of type A. However, given that $U_0 = 0$, and hence $F_0 = 0$, the type A wave generated with this procedure has a very limited domain of existence; in fact, we have $F_0\sqrt{\eta}/F_1 = 0$ and hence $-1 \leq \Delta/F_1 \leq 1$.

Experimental conditions and results are summarized in Table II; in the case of diffuse fronts, the wave speed is computed as the speed at which the average water depth (average between the wave front and toe) moves downstream. The flow velocity U_1 at the *vena contracta* cross section after the gate operation is estimated using Eq. (21) with $c_c = Y_1/w_1$.

To study the surge wave configurations of type A and D, a special device is adopted, which introduces an energy dissipation between a cross section just upstream of the gate and the *vena contracta* cross section; this energy dissipation is produced by a movable, very porous screen that partially obstructs the gate opening [Fig. 6(a)].

To produce the surge configuration of type A, starting from the free outflow conditions with the porous screen on place to close the

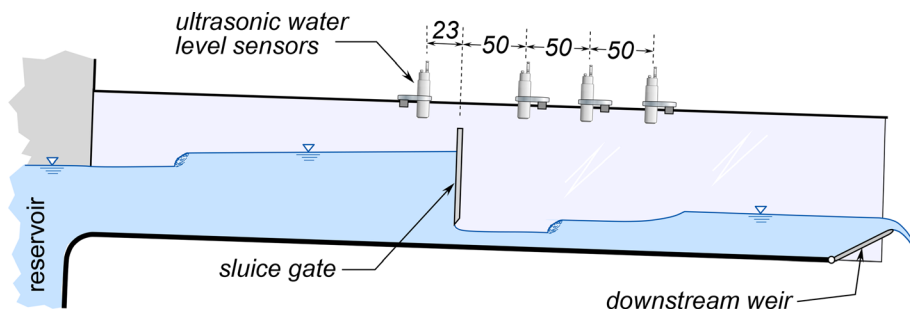


FIG. 5. Side view of the experimental setup. All dimensions are in centimeters.

TABLE II. Summary of the present experimental conditions and results of SET 1; P is the procedure, q_0 is the flow rate per unit width entering the flume, Y_0 is the undisturbed flow depth, Y_A and Y_B are the flow depths upstream of the gate before and after the gate operation, respectively, w_0 and w_1 are the gate openings before and after the gate operation, respectively, Y_1 is the flow depth at the *vena contracta* cross section after the gate operation and U_1 is the corresponding flow velocity estimated with Eq. (21), Y_2 is the intermediate flow depth, a_u and a_d are the speed of the upstream and downstream waves, respectively (*italics* is used to denote the speed of diffuse wave fronts).

RUN	P	Type	q_0 (m ² s ⁻¹)	Y_A (m)	Y_0 (m)	w_0 (m)	Y_B (m)	w_1 (m)	Y_1 (m)	U_1 (m s ⁻¹)	Y_2 (m)	a_u (m s ⁻¹)	a_d (m s ⁻¹)
1	4	A	0.0	0.238	0.025	0.000	0.186	0.062	0.041	1.73	0.088	0.50	1.50
2	4	A	0.0	0.199	0.025	0.000	0.150	0.062	0.041	1.49	0.080	0.36	1.33
3	4	A	0.0	0.222	0.069	0.000	0.176	0.062	0.037	1.70	0.120	0.66	1.34
4	4	A	0.0	0.334	0.028	0.000	0.310	0.025	0.018	2.23	0.090	0.60	1.42
5	3	B	0.049	0.352	0.023	0.030	0.280	0.128	0.083	2.06	0.048	<i>1.40</i>	2.78
6	3	B	0.040	0.256	0.020	0.030	0.175	0.128	0.085	1.52	0.034	<i>0.95</i>	2.50
7	3	B	0.017	0.116	0.013	0.020	0.090	0.062	0.030	1.15	0.017	<i>0.71</i>	1.70
8	3	B	0.013	0.175	0.008	0.012	0.129	0.062	0.040	1.39	0.018	<i>0.93</i>	2.00
9	3	B	0.020	0.135	0.013	0.020	0.097	0.062	0.038	1.16	0.019	<i>0.73</i>	1.90
10	1	C	0.101	0.182	0.061	0.100	0.249	0.022	0.014	2.15	0.043	1.03	2.38
11	1	C	0.069	0.203	0.037	0.060	0.239	0.022	0.014	2.10	0.027	1.33	2.24
12	1	C	0.094	0.215	0.050	0.080	0.275	0.015	0.009	2.29	0.032	1.37	2.38
13	2	C	0.066	...	0.105	...	0.155	0.035	0.021	1.63	0.087	0.10	<i>1.48</i>
14	2	C	0.064	...	0.077	...	0.144	0.035	0.022	1.58	0.065	0.32	<i>1.61</i>
15	2	C	0.063	...	0.067	...	0.122	0.050	0.031	1.41	0.061	0.39	<i>1.88</i>
16	2	C	0.082	...	0.083	...	0.175	0.030	0.020	1.61	0.062	0.44	<i>1.77</i>
17	2	C	0.082	...	0.083	...	0.165	0.030	0.019	1.59	0.061	0.43	<i>1.76</i>

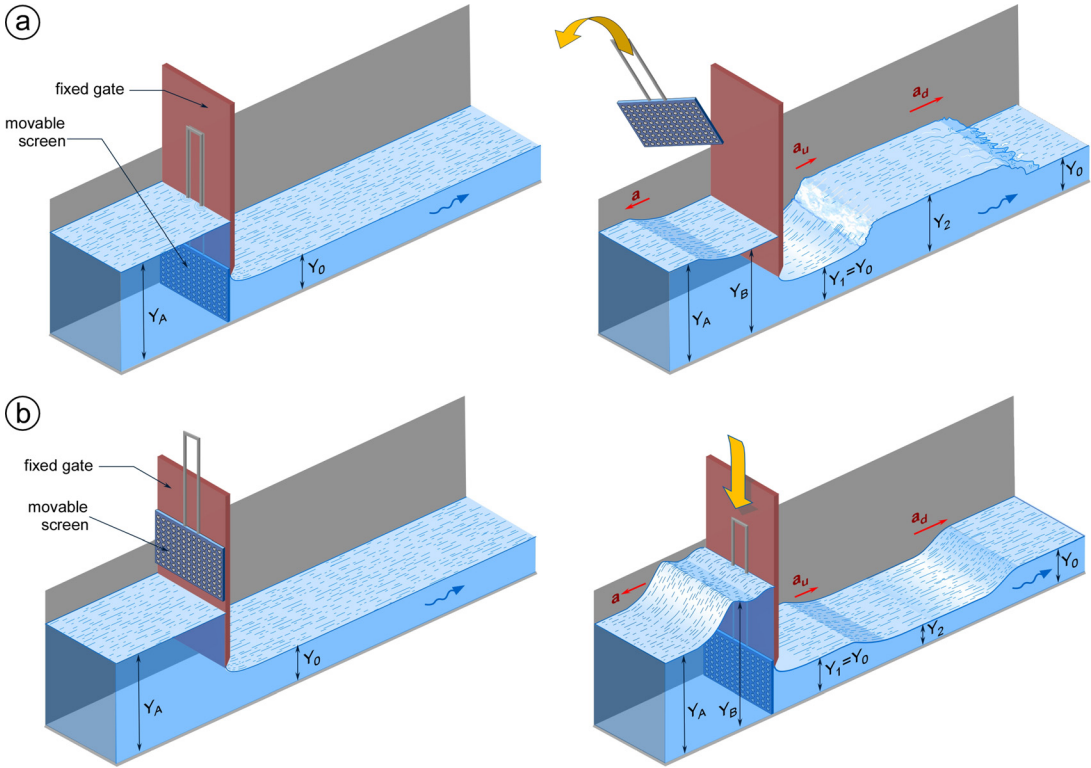


FIG. 6. (a) Device and procedure to generate a wave configuration of type A; a porous movable screen, initially placed to partially obstruct the sluice gate opening (left panel) is suddenly removed (right panel). (b) Device and procedure to generate a wave configuration of type D; starting from free outflow conditions (left panel), a porous movable screen is suddenly inserted upstream of the sluice gate to partially obstruct the gate opening (right panel).

gate opening, the screen is suddenly removed as shown in Fig. 6(a) (procedure 5).

On the contrary, to produce the surge configuration of type D, starting from the free outflow conditions, the screen is suddenly inserted to choke the gate opening as shown in Fig. 6(b) (procedure 6).

With the screen on place, and for any gate opening, w , the relationship between the flow rate and the water depth, Y_A , just upstream of the gate is determined experimentally under steady free outflow conditions. The energy conservation equation across the gate reads

$$Y_A + \frac{q^2}{2gY_A^2} - \Delta E = wc_c + \frac{q^2}{2g(wc_c)^2}, \quad (22)$$

with q being the flow rate per unit width, c_c being the contraction coefficient, and ΔE being the energy dissipated through the porous screen. By assuming

$$\Delta E = \alpha \frac{q^2}{2g(wc_c)^2} \approx \alpha(Y_A - wc_c), \quad (23)$$

with α being the calibration factor, Eq. (22) can be rewritten as

$$q = c_q w \sqrt{2gY_A} \quad \text{with} \quad c_q = \frac{c_c}{\sqrt{1 + \frac{\alpha Y_A + wc_c}{Y_A(1 - \alpha)}}}. \quad (24)$$

When the screen is rapidly inserted just upstream of the gate opening, as in the case shown in Fig. 6(b), the above Eqs. (22)–(24), with Y_B in place of Y_A , still hold.

Applying Eq. (24) to a large set of steady flow conditions with gate openings w , flow rates q , and flow depths upstream of the gate Y_A , in the range of values used in the experiments, we found $\alpha \approx 0.6$ independently from the flow rate and the gate opening.

The porous screen was also used in combination with specific gate operations to generate more varied conditions than those achievable by operating the gate alone.

By operating the sluice gate according to procedure 1, the wave configuration of type C can easily be generated; however, the generated flow configuration has necessarily $U_0 < U_1$, i.e., $F_0\sqrt{\eta}/F_1 < 1$ (see the experimental results of Montuori and Greco¹² presented in Fig. 7, later in the text). In order to generate flow configurations of type C with $U_0 > U_1$, the following procedure is adopted. Starting from the uniform flow conditions with depth Y_0 , the sluice gate is suddenly lowered to the opening w_1 and, simultaneously, the porous screen is inserted to choke the gate opening. This procedure is named procedure 2.6 since it combines procedures 2 and 6. As an alternative, the following procedure is adopted in the experiments. Starting from the free outflow conditions with the gate opening w_0 , the sluice gate is suddenly lowered to the opening $w_1 < w_0$ and, simultaneously, the porous screen is inserted to choke the gate opening. Since this procedure combines procedures 1 and 6, it is named procedure 1.6.

Similarly, by operating the sluice gate according to procedure 3, the wave configuration of type B can be generated; however, the generated flow configuration has necessarily $U_0 > U_1$, i.e., $F_0\sqrt{\eta}/F_1 > 1$ (see the experimental results of Montuori and Greco¹² presented in Fig. 7, later in the text). In order to generate flow configurations of type B with $U_0 < U_1$, the following procedure is adopted. Starting from the free outflow conditions with the gate opening w_0 and with

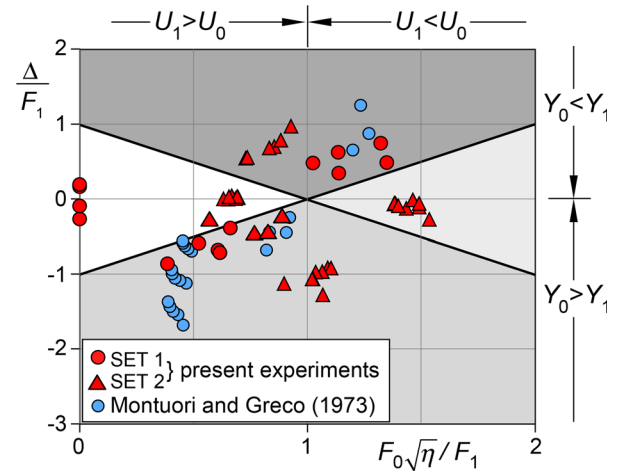


FIG. 7. Experimental conditions reported in the diagram with the theoretical domain of existence of the four possible surge wave configurations. The type of wave configuration found in the experiments was always predicted correctly by the proposed theoretical criterion.

the porous screen on place to choke the flow, the sluice gate is suddenly raised to the opening $w_1 > w_0$ and, simultaneously, the porous screen is removed. Since this procedure combines procedures 3 and 5, it is named procedure 3.5.

The experimental conditions and results are summarized in Table III; in the case of diffuse fronts, as for experiments of SET 1, the wave speed is the speed at which the average water depth (average between the wave front and toe) moves downstream.

On the whole, experimental conditions are such to cover the fields of existence of the four double surge configurations as succinctly shown in Fig. 7; here, experiments performed by Montuori and Greco¹² are distinguished from present experiments of SET 1 and from experiments of SET 2, in which the porous screen is used. Importantly, the proposed criterion to predict the wave configuration never failed.

Figure 8 shows some examples of the four surge wave configurations extracted from the recorded videos. The surge wave of type A is the easiest to observe since both waves have sharp fronts [Fig. 8(a)]. On the contrary, the wave configuration of type D is rather difficult to detect visually because both wave fronts are diffuse and the free surface profile is therefore very smooth; however, a close inspection of Fig. 8(d) reveals that the flow depth in the intermediate region is actually smaller than both upstream and downstream flow depths, thus confirming a D-type wave configuration.

Figure 9 shows some examples of the time evolution of water levels recorded by the four ultrasonic sensors as compared with model predictions. The upstream wave, which crosses the ultrasonic sensors at the later time, looks more diffuse than the downstream wave; this is because it takes a longer time to pass each ultrasonic sensor due to this lower speed.

It is important to stress that the upstream (Y_1) and downstream (Y_0) water levels, as well as water levels upstream of the sluice gates (Y_A and Y_B), are measured and prescribed as boundary conditions for the model; therefore, a significant comparison between theory and

TABLE III. Summary of the present experimental conditions and results of SET 2; P is the procedure, q_0 is the flow rate per unit width entering the flume, Y_0 is the undisturbed flow depth, Y_A and Y_B are the flow depths upstream of the gate before and after the gate operation, respectively, w_0 and w_1 are the gate openings before and after the gate operation, respectively, Y_1 is the flow depth at the *vena contracta* cross section after the gate operation and U_1 is the corresponding flow velocity estimated with Eq. (21), Y_2 is the intermediate flow depth, a_u and a_d are the speed of the upstream and downstream waves, respectively (*italics* is used to denote the speed of diffuse wave fronts).

RUN	P	Type	q_0 (m ² s ⁻¹)	Y_A (m)	Y_0 (m)	w_0 (m)	Y_B (m)	w_1 (m)	Y_1 (m)	U_1 (m s ⁻¹)	Y_2 (m)	a_u (m s ⁻¹)	a_d (m s ⁻¹)
1	5	A	0.033	0.171	0.031	0.050	0.153	0.050	0.032	1.53	0.045	0.80	1.81
2	5	A	0.046	0.307	0.032	0.050	0.293	0.050	0.033	2.21	0.057	1.36	2.34
3	5	A	0.057	0.407	0.034	0.050	0.393	0.050	0.033	2.59	0.062	1.60	2.73
4	5	A	0.043	0.250	0.032	0.050	0.235	0.050	0.032	1.97	0.052	1.20	2.14
5	5	A	0.044	0.242	0.036	0.062	0.220	0.062	0.039	1.86	0.055	0.96	2.14
6	5	A	0.043	0.228	0.035	0.062	0.212	0.062	0.039	1.82	0.055	0.94	2.14
7	5	A	0.039	0.193	0.034	0.062	0.176	0.062	0.037	1.64	0.052	0.81	1.97
8	5	A	0.056	0.407	0.034	0.050	0.393	0.050	0.034	2.58	0.063	1.53	2.68
9	5	A	0.048	0.277	0.036	0.062	0.260	0.062	0.040	2.04	0.057	1.11	2.25
10	1.5	A	0.035	1.277	0.033	0.053	0.187	0.020	0.012	1.86	0.038	0.86	1.67
11	3.5	B	0.023	0.355	0.014	0.020	0.270	0.128	0.082	2.02	0.050	1.36	2.73
12	3.5	B	0.020	0.262	0.015	0.019	0.168	0.128	0.087	1.48	0.043	0.77	2.38
13	3.5	B	0.008	0.145	0.008	0.012	0.096	0.062	0.040	1.15	0.022	0.70	1.76
14	3.5	B	0.009	0.205	0.008	0.012	0.162	0.062	0.040	1.60	0.027	1.01	2.08
15	3.5	B	0.009	0.196	0.008	0.012	0.149	0.062	0.039	1.52	0.031	0.96	1.95
16	3.5	B	0.023	0.351	0.014	0.019	0.265	0.128	0.081	2.00	0.050	1.33	2.73
17	1.6	C	0.087	0.148	0.064	0.100	0.210	0.018	0.012	1.25	0.031	0.54	1.63
18	1.6	C	0.090	0.149	0.065	0.100	0.218	0.008	0.006	1.55	0.025	0.51	1.53
19	1.6	C	0.087	0.150	0.062	0.100	0.215	0.018	0.011	1.27	0.030	0.59	1.70
20	1.6	C	0.087	0.151	0.064	0.100	0.215	0.008	0.007	1.28	0.025	0.56	1.58
21	2.6	C	0.085	...	0.070	...	0.177	0.025	0.015	1.13	0.036	0.37	1.58
22	2.6	C	0.084	...	0.071	...	0.180	0.025	0.015	1.14	0.036	0.39	1.60
23	2.6	C	0.101	...	0.081	...	0.203	0.025	0.015	1.22	0.042	0.39	1.60
24	2.6	C	0.101	...	0.081	...	0.203	0.025	0.015	1.22	0.042	0.39	1.60
25	1.6	D	0.049	0.182	0.030	0.047	0.192	0.032	0.022	1.16	0.014	0.79	1.95
26	1.6	D	0.083	0.403	0.030	0.047	0.435	0.018	0.010	1.83	0.005	1.56	2.83
27	1.6	D	0.051	0.180	0.029	0.047	0.194	0.032	0.023	1.17	0.014	0.79	2.00
28	6	D	0.057	0.145	0.039	0.062	0.169	0.062	0.035	1.05	0.025	0.55	1.88
29	6	D	0.057	0.200	0.032	0.050	0.215	0.050	0.031	1.21	0.018	0.82	2.05
30	6	D	0.056	0.198	0.031	0.050	0.212	0.050	0.027	1.21	0.016	0.87	2.09
31	6	D	0.057	0.145	0.039	0.062	0.168	0.062	0.035	1.04	0.025	0.59	1.91
32	6	D	0.067	0.189	0.040	0.062	0.213	0.062	0.035	1.20	0.023	0.71	2.00
33	6	D	0.042	0.118	0.033	0.050	0.133	0.050	0.030	0.92	0.022	0.52	1.65
34	6	D	0.053	0.131	0.038	0.062	0.154	0.062	0.032	1.00	0.024	0.60	1.79

experiments only considers the water depth of the intermediate region (Y_2) and the speed of the two wave fronts (i.e., the temporal position of the two wave fronts in the t - Y diagram).

It is also important to recall that the discussion on comparison between experimental and theoretical results must be done with due care because of the impact of the transient phase on the surge wave generation. For example, when the gate is quickly lifted as in the case shown in Fig. 8(b), due to inertia, the amplitude of the negative wave produced upstream of the gate is greater than predicted and it is followed by a positive shock migrating upstream; as a result, the water level upstream of the gate oscillates around its steady position (see, e.g., the lower central panel of Fig. 9), affecting the downstream flow. The

opposite occurs when the gate is suddenly lowered as for the case shown in Fig. 8(c). In this case, the upstream positive shock wave has a height greater than predicted and the water level upstream of the gate oscillates around its steady position (see, e.g., the upper right panel of Fig. 9), here too affecting the downstream flow.

Figure 10 compares the experimental relative depth of the intermediate flow, Y_2/Y_0 , and the relative speed of the upstream and downstream wave fronts, a_u/c_0 , a_d/c_0 ($c_0 = \sqrt{gY_0}$), with model predictions; the agreement is very good for all three variables, with the largest errors that remain smaller than $\pm 10\%$ anyway.

The R^2 value for model prediction of the intermediate flow depth, Y_2 , and of the upstream wave speed, a_u , is $R^2 = 0.99$, whereas R^2

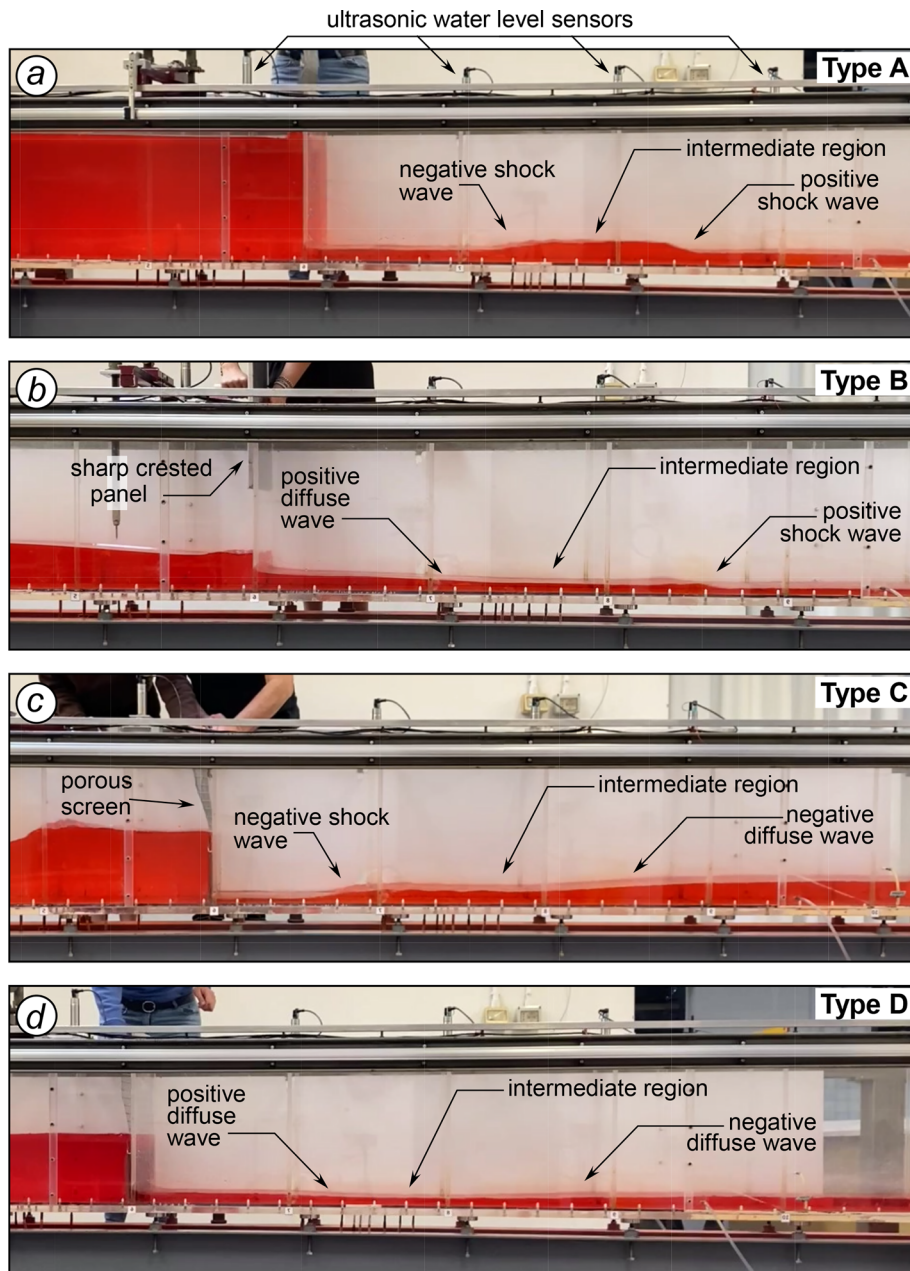


FIG. 8. Frames from recorded videos showing the four double surge systems generated by a supercritical flow suddenly entering upstream of a preexisting current: (a) wave configuration of type A generated with procedure 5 and position of the four ultrasonic water level sensors, (b) wave configuration of type B generated with procedure 3, (c) wave configuration of type C generated with procedure 1.6, and (d) wave configuration of type D generated with procedure 6. The flow is from left to right.

reduces to $R^2 = 0.97$ for model prediction of the downstream wave speed. Prediction of a_d is less accurate, possibly because the downstream wave quickly moves away from where it is generated, while flow conditions at the gate are not quasi-steady yet.

A further set of experiments is performed (SET 3), in which conditions are such that the upstream surge wave does not propagate and remains on place. In particular, procedure 4 is used to generate a surge wave system of type Aw, whereas procedure 2 is used to generate the flow configuration of type Cw; in both cases, the flow through the sluice gate becomes submerged and hence the upstream wave is stopped by the gate that generates the upstream supercritical current.

It is worth recalling that in this case the flow configuration is described by model Eqs. (19) and (20), with $Y_1 = w_1 c_c$ and U_1 estimated as described in Appendix B.

Experimental conditions and results of this set of experiments are given in Table IV. Figure 11 compares model prediction with experimental results; the agreement is generally very good for the intermediate flow depth, Y_2 , whereas only a moderate accuracy can be observed in the comparison between theoretical and experimental speed of the downstream wave, a_d , with an error that remains smaller than $\pm 10\%$ anyway. Importantly, all experiments confirmed that the upstream wave does not propagate downstream when $F_1 < F_1^*$.

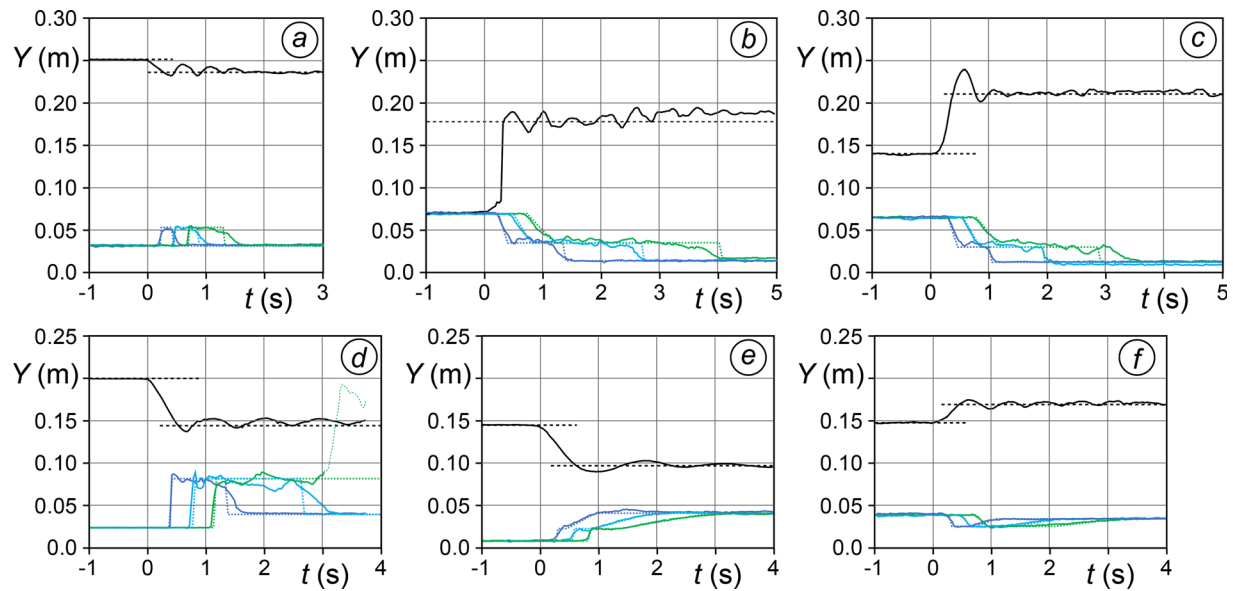


FIG. 9. Examples of time evolution of water levels recorded by the four ultrasonic sensors (solid lines) as compared with model predictions (dashed lines). (a) Configuration A, procedure 5, (b) configuration C, procedure 2.6, (c) configuration C, procedure 1.6, (d) configuration A, procedure 4, (e) configuration B, procedure 3.5, and (f) configuration D, procedure 6. Black lines denote the water level at the upstream ultrasonic sensor; blue, cyan, and green lines denote the downstream ultrasonic water level sensors located at distances 0.5, 1.0, and 1.5 m from the sluice gate, respectively; time $t = 0$ corresponds to the moment when the operation at the gate is performed.

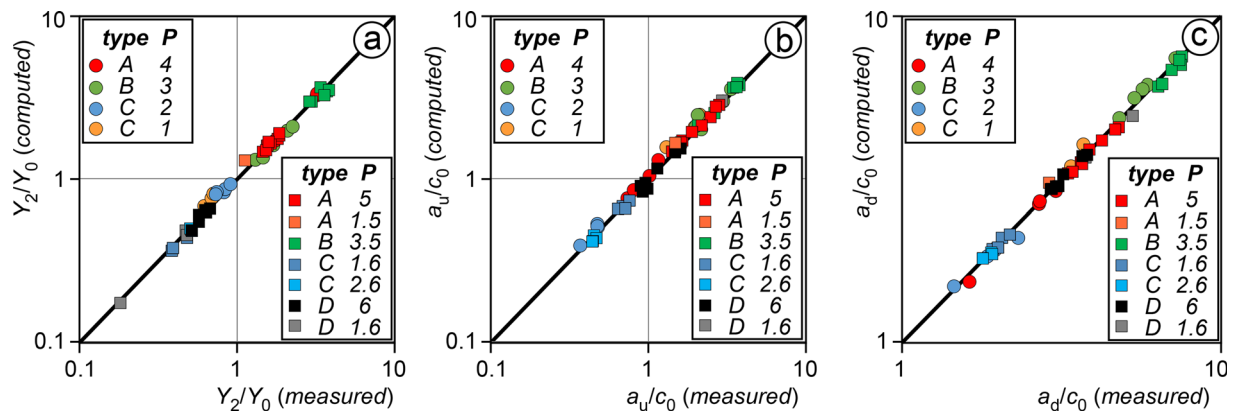


FIG. 10. Comparison between the measured and computed (a) relative depth of the intermediate flow, Y_2/Y_0 , (b) the relative speed of the upstream wave, a_u/c_0 , and (c) the relative speed of the downstream wave, a_d/c_0 , with $c_0 = \sqrt{gY_0}$. All plots are in log-log scale. Circles and squares distinguish results of SET 1 and SET 2 experiments, respectively.

B. Numerical investigations

A large number of numerical simulations are performed to reproduce the conditions for the development of the four surge wave configurations, for both the cases of supercritical or subcritical undisturbed flow; in particular, all the laboratory experiments are simulated with the numerical model to further check the correctness and reliability of the theoretical model. Some additional examples of practical interest are also presented and discussed.

1. The numerical model

A standard Godunov-type finite volume method on unstructured triangular grids is used to solve the SWEs.⁵ Although a one-dimensional

model could confidently be used, a two-dimensional model is used simply because available.

Bottom elevation is defined at the grid nodes and assumed to vary linearly within each cell of the mesh to describe sloping channels and sudden variations of the bed with a second-order accuracy.^{3,19,20} Variables are reconstructed at cell faces using the adaptive scheme of Begnudelli *et al.*,⁴ in which the local Froude number determines the selection of either primitive or conservative variables to avoid the generation of unphysical discontinuities. Water and momentum fluxes at the cell sides are then evaluated using the Exact Riemann Solver proposed by Toro.¹⁵ The bed friction is evaluated with the Manning formula, and the slip condition is assumed at the lateral walls of the domain. Such a first-order adaptive scheme with a second-order

TABLE IV. Summary of SET 3 experimental conditions and results; P is the procedure, q_0 is the flow rate per unit width entering the flume, Y_0 is the undisturbed flow depth, Y_A and Y_B are the flow depths upstream of the gate before and after the gate operation, respectively, w_0 and w_1 are the gate openings before and after the gate operation, respectively, $Y_1 = w_1 c_c$ is the thickness of the *vena contracta* after the gate operation and U_1 is the corresponding flow velocity estimated as described in Appendix B, Y_2 is the intermediate flow depth, a_d is the speed of the downstream wave (italics is used to denote the speed of diffuse wave fronts).

RUN	P	Type	q_0 (m ² s ⁻¹)	Y_A (m)	Y_0 (m)	w_0 (m)	Y_B (m)	w_1 (m)	Y_1 (m)	U_1 (m s ⁻¹)	Y_2 (m)	a_d (m s ⁻¹)
1	4	Aw	0.0	0.229	0.108	0.000	0.194	0.062	0.034	1.31	0.146	1.28
2	4	Aw	0.0	0.186	0.065	0.000	0.164	0.025	0.016	1.58	0.087	1.05
3	4	Aw	0.0	0.203	0.102	0.000	0.169	0.062	0.033	1.12	0.137	1.20
4	4	Aw	0.0	0.277	0.121	0.000	0.260	0.025	0.015	1.72	0.143	1.20
5	4	Aw	0.0	0.235	0.127	0.000	0.220	0.025	0.014	1.36	0.144	1.14
6	2	Cw	0.069	...	0.130	...	0.175	0.035	0.022	1.56	0.105	1.50
7	2	Cw	0.069	...	0.130	...	0.175	0.035	0.022	1.56	0.103	1.46
8	2	Cw	0.067	...	0.151	...	0.187	0.032	0.019	1.39	0.126	1.50
9	2	Cw	0.033	...	0.158	...	0.182	0.010	0.006	0.97	0.138	1.30
10	2	Cw	0.082	...	0.157	...	0.225	0.010	0.006	1.44	0.108	1.36
11	2	Cw	0.051	...	0.152	...	0.180	0.032	0.019	1.14	0.135	1.40
12	2	Cw	0.034	...	0.158	...	0.173	0.032	0.018	0.85	0.147	1.33
13	2	Cw	0.051	...	0.156	...	0.194	0.010	0.059	1.22	0.125	1.32
14	2	Cw	0.068	...	0.156	...	0.205	0.010	0.006	1.26	0.115	1.38
15	2	Cw	0.100	...	0.158	...	0.244	0.010	0.006	1.99	0.102	1.46

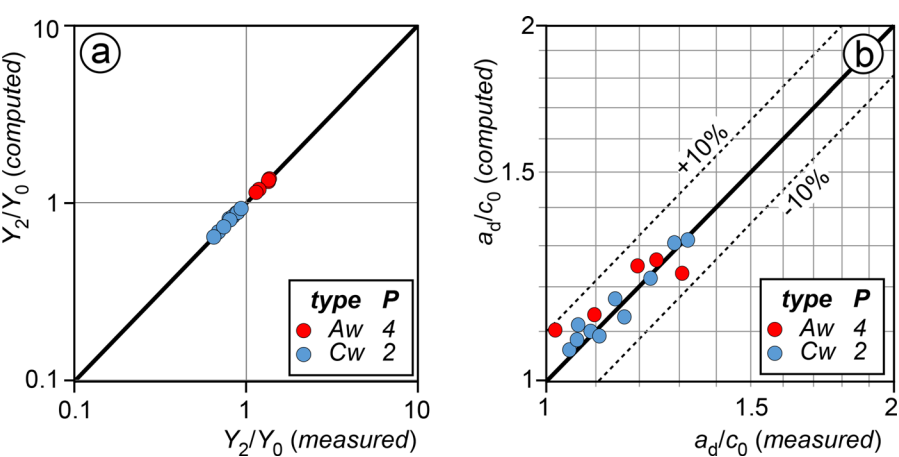


FIG. 11. Comparison between the measured and theoretically estimated (a) relative depth of the intermediate flow, Y_2/Y_0 , and (b) relative speed of the downstream wave, a_d/c_0 , with $c_0 = \sqrt{gY_0}$. All plots are in log-log scale.

accurate bed description was shown to be robust, efficient, and accurate for many engineering applications including flow fields with shock and diffuse waves.^{4,6,21}

In the present study, the flow on long channels with either horizontal or sloping beds is reproduced by progressively increasing the mesh resolution until the solution becomes independent of the grid.

2. Numerical results with discussion

Some of the cases pertaining to SET 1 and SET 2, as well as some cases of SET 3, solved theoretically, have been simulated with the numerical model starting from the given undisturbed flow conditions Y_0 and U_0 and by prescribing an instantaneous variation of the upstream flow depth and velocity, Y_1 and U_1 , as boundary conditions. Bed friction is neglected. The good agreement between the numerical

results and the theoretical predictions definitely suggests that the proposed theoretical model can comfortably be used to predict the main characteristics of the phenomenon at hand. In addition, here below are described and discussed some simulations of the double surge wave system that develops under different conditions of practical interest that cannot be easily reproduced in the lab.

Example 1. As stated in the Introduction, the double surge wave system can be generated by the sudden release of discharges in an open channel receiving tailwater, downstream of a dam or a hydro-power plant; the present example simulates this situation. It uses a straight channel of unit width in which a constant rate tailwater flows down the steep upper reach of the channel and meets the still water in the horizontal downstream reach of channel. The bed slope of the upstream reach of the channel is $s = 5\%$, and the friction coefficient in the Manning formula is $n = 0.02 \text{ m}^{-1/3} \text{ s}$. Initial conditions consist of

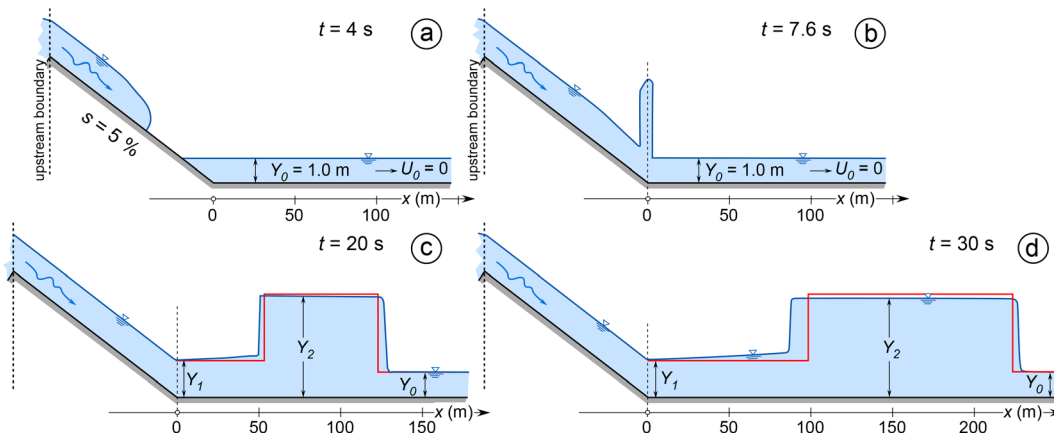


FIG. 12. Example 1. (a) Flow configuration just before the incoming supercritical current hits the downstream still water. (b) The free surface spike generated by the collision of the two currents about $x = 0$. (c) The double surge wave system at $t = 20$ s and (d) the same at $t = 30$ s; the red profiles show the theoretical solution.

still water, with depth $Y_0 = 1.0$ m, in the downstream reach of the channel, whereas the steep reach of the channel is initially dry. A flow rate $q = 20 \text{ m}^2 \text{ s}^{-1}$ with a water depth of 1.5 m, both constant in time, is prescribed as upstream boundary conditions, whereas the water depth $Y_0 = 1.0$ m is prescribed far downstream [Fig. 12(a)].

With the above data, we have $Y_1 \approx 1.5$ m, $\eta \approx 0.667$, $\Delta \approx 0.37$, $F_0 = 0$, and $U_1 \approx 13$ m/s so that $F_1 \approx 3.4$; we then have $F_0\sqrt{\eta}/F_1 = 0$ and $\Delta/F_1 \approx 0.266$, and hence, a double surge system of type A is expected. In addition, using Eqs. (15) and (16), we find $F_1^* \approx 1.4 < F_1$ so that both surge waves are expected to migrate downstream.

At $t \approx 7.6$ s, the incoming, supercritical flow reaches the downstream still water and generates a spike of the free surface that rises quickly [Fig. 12(b)]; this spike is actually the new born double surge wave of type A.

Figures 12(c) and 12(d) compare the numerical results with the predictions of the theoretical model at $t = 20$ and $t = 30$ s, respectively. Discrepancies are moderately small and are mainly due to bed friction, which is neglected in the theoretical model. The free surface between the two surges, as predicted by the numerical model, is nearly horizontal; this is because the flow velocity (and hence the bed friction) is relatively small if compared to U_1 ($U_2 = 7.4$ m/s according to the numerical model and $U_2 = 7.5$ m/s according to the theory).

Example 2. This example uses the same geometry and initial conditions of example 1. A flow rate $q = 0.8 \text{ m}^2 \text{ s}^{-1}$ with a water depth of 0.2 m, both constant in time, is prescribed as upstream boundary conditions, whereas the water depth $Y_0 = 1.0$ m is prescribed at the downstream end of the channel.

In this case, we have $U_1 = 4$ m/s, $F_1 \approx 2.9$, and $F_1^* \approx 5.2 > F_1$ so that only the downstream wave travels downstream with a speed $a_d = 3.64$ m/s according to the theoretical model [i.e., Eq. (20)]. Moreover, according to the theory [i.e., Eqs. (19) and (20)], the flow depth and the velocity upstream of the wave front are $Y_2 = 1.22$ m and $U_2 = 0.65$ m/s, respectively.

The results of the numerical simulation are summarized in Fig. 13, showing the free surface profiles at some time instants; the surge wave speed is $a_d \approx 3.8$ m/s, and the flow depth and the velocity upstream of the wave front are $Y_2 = 1.22$ m and $U_2 = 0.63$ m/s, respectively. These results compare favorably well with the theory.

Example 3. This example uses a tail tunnel that ends in an open channel [Fig. 14(a)]. The tunnel and the channel share the same wide rectangular cross section; the tunnel has a flat ceiling of height $H = 1.0$ m. The channel bed slope is $s = 0.02$, and the bottom friction is computed by the Manning formula with a Manning coefficient $n = 0.018 \text{ s m}^{1/3}$. Initial conditions consist of a uniform flow, with depth $Y_0 = 1.0$ m and velocity $U_0 = 8$ m/s; the uniform pressure flow in the tunnel is not explicitly simulated by the numerical model, which only includes the downstream open channel. Starting from these conditions, the flow rate in the tunnel is quickly reduced to $q_1 = 4 \text{ m}^2/\text{s}$ (e.g., by operating an outlet control valve), while keeping the flow depth $H = Y_1 = 1.0$ m so that $U_1 = 4$ m/s; radiation conditions are prescribed at the downstream end of the channel.

In this case, we have $\eta = 1.0$ and hence $\Delta = 0$, $F_0 = 2.55$, and $F_1 = 1.28$; we then have $F_0\sqrt{\eta}/F_1 = 2.0$ and $\Delta/F_1 = 0$; according to the proposed criterion, a double surge wave system of type D is expected.

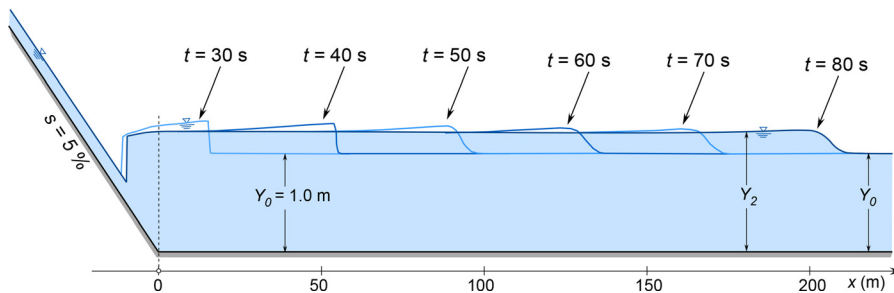


FIG. 13. Example 2. Free surface profiles at different times showing the downstream wave propagating with a speed $a_d \approx 3.8$ m/s, whereas the upstream wave remains on place.

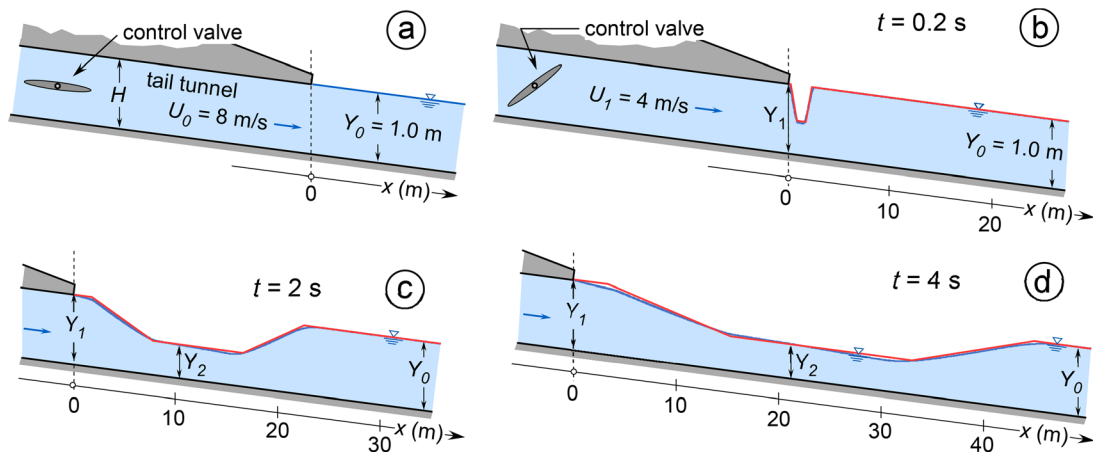


FIG. 14. Example 3. (a) Flow configuration just before operating the outlet control valve; the flow is uniform, with depth $Y_0 = 1.0$ m and velocity $U_0 = 8$ m/s. (b) The negative free surface spike generated 0.2 s after the sudden partial closure of the control valve so that the upstream flow velocity is reduced to $U_1 = 4$ m/s. (c) The double surge wave system of type D at $t = 2$ s and (d) the same at $t = 4$ s; the red profiles show the theoretical solution.

The results provided by the numerical model, which compare favorably well with the theory, show that a double surge wave of type D develops just after the outlet control valve is partly closed [Fig. 14(b)]; this wave propagates downstream with both the negative and positive fronts that gradually expand as shown in Figs. 14(c) and 14(d). It is worth pointing out that, to draw the theoretical water surface profile, we evaluated (at time $t = 0.2$, $t = 2$, and $t = 4$ s) the position of the head and of the toe of both the upstream and the downstream diffuse waves and assumed that water depth approximately varies linearly between the two ends of each wave.

IV. CONCLUSIONS

When a supercritical flow rapidly enters from upstream a pre-existing uniform current, a system of two waves develops; the combination of positive and negative waves, as well as of shock or diffuse waves, leads to four possible double surge wave configurations.

In the present study, the theoretical model by Montuori¹¹ has been improved by including the cases when the upstream wave remains stuck at the upstream section where these waves are generated. A new criterion, to distinguish between the four double surge wave configurations, has been proposed, which is based only on the undisturbed flow characteristics and on conditions forcing the wave generation.

Ad hoc laboratory experiments have been designed and performed to test the theoretical model. The combined use of a vertical sluice gate and of a porous screen allowed to generate all the four double wave configurations, including the cases when the upstream wave remains stuck at the upstream section.

The predictions of the theoretical model have been compared also with the results of a numerical model solving the shallow water equations that allowed analyzing further cases of practical interest, such as the sudden variation of the tailwater downstream of control structures, which are more difficult to be reproduced in the lab.

The good agreement between laboratory, numerical, and theoretical results confirmed, on one hand, the good predictive ability of the theoretical model and, on the other hand, that the shallow water approximation can capture the salient features of the unsteady processes here investigated.

As future work, it could be interesting to investigate the wave system developing when the upstream supercritical flow is introduced nearby a more complex geometrical configuration (e.g., channel width variation, misaligned inflow, etc.), which could be of practical interest. In such cases, three-dimensional numerical models^{1,2,7,10,14,17} could be necessary since both shock wave reflections and non-hydrostatic pressure are expected to significantly affect the flow field.

ACKNOWLEDGMENTS

I wish to acknowledge Letizia Croceri and Marianna Palleri for their contribution to the experimental and numerical investigations. I also thank Daniele Viero and Luca Cozzolino for the fruitful discussion.

AUTHOR DECLARATIONS

Conflict of Interest

The authors have no conflicts to disclose.

Author Contributions

Andrea Defina: Conceptualization (equal); Data curation (equal); Formal analysis (equal); Investigation (equal); Methodology (equal); Project administration (equal); Resources (equal); Software (equal); Supervision (equal); Validation (equal); Visualization (equal); Writing – original draft (equal).

DATA AVAILABILITY

The data that support the findings of this study are openly available in Research Data Unipd at <https://researchdata.cab.unipd.it/id/eprint/1108>, Ref. 22.

NOMENCLATURE

a	Wave speed (m s^{-1})
c_c	Sluice gate contraction coefficient (–)
c_q	Sluice gate discharge coefficient (–)
F	Froude number (–)

- n Manning friction coefficient ($\text{m}^{-1/3} \text{s}$)
- q Flow rate per unit width ($\text{m}^2 \text{s}^{-1}$)
- s Channel bed slope ($-$)
- U Flow velocity (m s^{-1})
- w Sluice gate opening (m)
- Y Flow depth (m)
- η Flow depth ratio Y_0/Y_1
- θ Flow depth ratio Y_2/Y_1

APPENDIX A: ITERATIVE SOLUTION OF MODEL EQUATIONS

The set of Eqs. (1), (3), (5), and (6) is solved iteratively. Starting from the first guess for Y_2 , e.g., $Y_2 = Y_1$,

- (i) a_u is computed with Eq. (5), and a_d is computed with Eq. (6);
- (ii) the velocity U_2 , labeled U_{2u} , is solved from Eq. (1);
- (iii) similarly, the velocity U_2 , labeled U_{2d} , is solved from Eq. (3);
- (iv) the correction factor, $\Delta Y = Y_1(U_{2u} - U_{2d})/(a_u + a_d)$, is computed
- (v) the new guess for Y_2 is found by adding ΔY to the previously guessed Y_2 .

The process, i.e., points (i)–(v), is repeated until convergence. Once convergence is achieved, all variables of the problem can be easily updated.

Equation (19) can be solved iteratively. A first guess for Y_2 , e.g., $Y_2 = Y_1$, must be put into the right side of Eq. (19), and the new guess for Y_2 is explicitly given by the left side of the equation. The procedure is repeated until convergence.

APPENDIX B: THE CASE OF SUBMERGED FLOW

To determine the flow velocity U_1 when the flow through the sluice gate is submerged, the full flow configuration generated by the gate operation must be resolved.

Figure 15 shows the flow configurations of type Aw, generated with procedure 4, and of type Cw generated with procedure 2, with notations; the approach to solve these flow configurations is basically the same.

In the frame reference of the surge generating upstream of the gate, the mass and momentum balance equations across the surge can be written as

$$(U_A - a_0)Y_A = (U_B - a_0)Y_B, \quad (\text{B1})$$

$$\frac{Y_A^2}{2} + \frac{(U_A - a_0)^2 Y_A}{g} = \frac{Y_B^2}{2} + \frac{(U_B - a_0)^2 Y_B}{g}. \quad (\text{B2})$$

Similarly, in the frame reference of the downstream surge, the mass and momentum balance equations across the surge can be written as

$$(U_2 - a_d)Y_2 = (U_0 - a_d)Y_0, \quad (\text{B3})$$

$$\frac{Y_2^2}{2} + \frac{(U_2 - a_d)^2 Y_2}{g} = \frac{Y_0^2}{2} + \frac{(U_0 - a_d)^2 Y_0}{g}. \quad (\text{B4})$$

Energy and momentum balance equations, respectively, across and just downstream of the gate, are written as

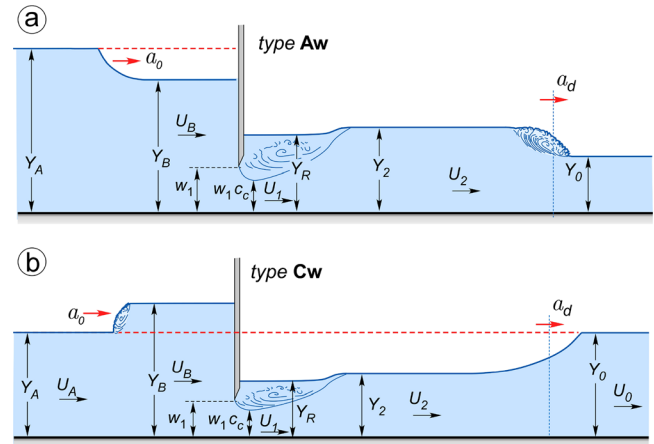


FIG. 15. (a) Flow configuration of type Aw, generated with the procedure 4, and (b) flow configuration of type Cw generated with the procedure 2 (b).

$$Y_B + \frac{U_B^2}{2g} = Y_R + \frac{U_1^2}{2g}, \quad (\text{B5})$$

$$\frac{Y_R^2}{2} + \frac{U_1^2 w_1 c_c}{g} = \frac{Y_2^2}{2} + \frac{U_2^2 Y_2}{g}. \quad (\text{B6})$$

Finally, mass conservation requires

$$U_B Y_B = U_1 w_1 c_c = U_2 Y_2. \quad (\text{B7})$$

The above set of eight equations can be solved for Y_B , Y_R , Y_2 , U_B , U_1 , U_2 , a_0 , and a_d once Y_A , U_A , Y_0 , U_0 , w_1 , and c_c are given. It is worth recalling that procedure 4 to generate the flow configuration of type Aw [Fig. 15(a)] requires $U_A = U_0 = 0$, whereas procedure 2 to generate the flow configuration of type Cw [Fig. 15(b)] requires $Y_A = Y_0$.

APPENDIX C: UNDISTURBED FLOW CONDITIONS SO THAT THE D-TYPE WAVE CONFIGURATION CAN DEVELOP

The double surge wave configuration of type D develops when both the below constraints are fulfilled

$$F_1 < F_0 \sqrt{\eta} + \Delta \quad \text{and} \quad F_1 < F_0 \sqrt{\eta} - \Delta.$$

The above constraints are rewritten as

$$F_0 > \frac{F_1 - \Delta}{\sqrt{\eta}} \quad \text{and} \quad F_0 > \frac{F_1 + \Delta}{\sqrt{\eta}},$$

or, equivalently

$$F_0 > \max \left\{ \frac{F_1 - \Delta}{\sqrt{\eta}}, \frac{F_1 + \Delta}{\sqrt{\eta}} \right\}. \quad (\text{C1})$$

To show that, for this wave configuration to develop, the undisturbed flow must be supercritical, i.e., $F_0 > 1$, it is sufficient to show that the constraint (C1) is fulfilled if and only if $F_0 > 1$.

Let us consider the case when $\eta = Y_0/Y_1 < 1$, and hence, $\Delta = (1 - \eta) \sqrt{(1/\eta + 1)/2} > 0$; the constraint (C1) reduces to

$$F_0 > \frac{F_1 + \Delta}{\sqrt{\eta}}.$$

At the numerator, $F_1 > 1$ and $\Delta > 0$ so that the numerator is greater than one. At the denominator, $\sqrt{\eta}$ is smaller than one so that, on the whole, we have $F_0 > 1$.

Let us consider the case when $\eta < 1$, and hence, $\Delta < 0$, and show that the first constraint is fulfilled only if $F_0 > 1$.

Let us consider the case when $\eta = Y_0/Y_1 > 1$, and hence, $\Delta = (1 - \eta)\sqrt{(1/\eta + 1)/2} < 0$; the constraint (C1) reduces to

$$F_0 > \frac{F_1 - \Delta}{\sqrt{\eta}}, \quad \text{i.e.,} \quad F_0 > \frac{F_1 + (\eta - 1)\sqrt{\frac{1}{2}\left(1 + \frac{1}{\eta}\right)}}{\sqrt{\eta}}.$$

The right-hand term increases with F_1 ; therefore, it is enough to show that $F_0 > 1$ when $F_1 = 1$, that is,

$$F_0 > \frac{1 + (\eta - 1)\sqrt{\frac{1}{2}\left(1 + \frac{1}{\eta}\right)}}{\sqrt{\eta}} > 1.$$

The right-hand constraint can be rewritten as

$$(\eta - 1)\sqrt{\eta + 1} > \sqrt{2\eta}(\sqrt{\eta} - 1),$$

and it can be further simplified to read

$$(\sqrt{\eta} + 1)\sqrt{\eta + 1} > \sqrt{2\eta}.$$

Since $\eta > 1$, the term on the left, between brackets, is greater than two, i.e., $(\sqrt{\eta} + 1)\sqrt{\eta + 1} > 2\sqrt{\eta + 1}$; hence, we can write

$$(\sqrt{\eta} + 1)\sqrt{\eta + 1} > 2\sqrt{\eta + 1} > \sqrt{2\eta}.$$

The above constraint is always fulfilled, confirming that $F_0 > 1$.

REFERENCES

- ¹Ai, C., Ma, Y., Ding, W., Xie, Z., and Dong, G., "An efficient three-dimensional non-hydrostatic model for undular bores in open channels," *Phys. Fluids* **33**, 127111 (2021).
- ²Ai, C., Ma, Y., Ding, W., Xie, Z., and Dong, G., "Three-dimensional non-hydrostatic model for dam-break flows," *Phys. Fluids* **34**, 022105 (2022).
- ³Begnudelli, L. and Sanders, B. F., "Unstructured grid finite-volume algorithm for shallow-water flow and scalar transport with wetting and drying," *J. Hydraul. Eng.* **132**(4), 371–384 (2006).
- ⁴Begnudelli, L., Sanders, B. F., and Bradford, S. F., "Adaptive Godunov-based model for flood simulation," *J. Hydraul. Eng.* **134**(6), 714–725 (2006).
- ⁵Defina, A., Susin, F. M., and Viero, D. P., "Numerical study of the Guderley and Vasilev reflections in steady two-dimensional shallow water flow," *Phys. Fluids* **20**(9), 097102 (2008).
- ⁶Defina, A. and Viero, D. P., "Open channel flow through a linear contraction," *Phys. Fluids* **22**(3), 036602 (2010).
- ⁷Gao, Y., Yang, H., Wang, L., and Zhao, M., "Three-dimensional numerical investigation on flow behaviors around a diversion dike," *Phys. Fluids* **34**, 125119 (2022).
- ⁸Henderson, F. M., *Open Channel Flow* (MacMillan Publishing Co., NY, 1966), pp. 67–75.
- ⁹Lazzarin, T., Viero, D. P., Defina, A., and Cozzolino, L., "Flow under vertical sluice gates: Flow stability at large gate opening and disambiguation of partial dam-break multiple solutions," *Phys. Fluids* **35**, 024114 (2022).
- ¹⁰Li, Z., Liu, C., Wan, D., and Hu, C., "High-fidelity simulation of a hydraulic jump around a surface-piercing hydrofoil," *Phys. Fluids* **33**, 123304 (2021).
- ¹¹Montuori, C., "Brusca immissione di una corrente ipercritica a tergo di altra preesistente," *Energ. Elett.* **XLV**(3), 174–187 (1968) (in Italian).
- ¹²Montuori, C. and Greco, V., "Fenomeni di moto vario a valle di una paratoia piana," *Energ. Elett.* **50**(2), 73–88 (1973) (in Italian).
- ¹³Rouse, H., *Elementary Mechanics of Fluid* (John Wiley & Sons, NY, 1946).
- ¹⁴Simon, B., Lubin, P., and Chanson, H., "Hydrodynamic shock in rivers: Physical and numerical modeling of flow structures in tsunami-like bores," *Phys. Fluids* **35**, 106607 (2023).
- ¹⁵Toro, E. F., *Shock-Capturing Methods for Free-Surface Shallow Flows* (John Wiley & Sons, 2001).
- ¹⁶Chow, V., *Open-Channel Hydraulics* (McGraw-Hill Civil Engineering Series, NY, 1959), pp. 554–567.
- ¹⁷Venkateshwaran, A., Li, Z., and Karimpour, S., "Turbulent characteristics and anisotropy in breaking surge waves: A numerical study," *Phys. Fluids* **35**, 015132 (2023).
- ¹⁸Viero, D. P., Pradella, I., and Defina, A., "Free surface waves induced by vortex shedding in cylinder arrays," *J. Hydraul. Res.* **55**(1), 16–26 (2017).
- ¹⁹Viero, D. P., Peruzzo, P., and Defina, A., "Positive surge propagation in sloping channels," *Water* **9**(7), 518 (2017).
- ²⁰Viero, D. P. and Defina, A., "Consideration of the mechanisms for tidal bore formation in an idealized planform geometry," *Water Resour. Res.* **54**, 5670–5686, <https://doi.org/10.1029/2018WR022937> (2018).
- ²¹Viero, D. P., Lazzarin, T., Peruzzo, P., and Defina, A., "Supercritical flow overpassing forward- or backward-facing steps non-orthogonal to the flow direction," *Phys. Fluids* **35**, 036604 (2023).
- ²²Dataset: A. Defina (2023). "Data of the double surge wave system that develops when a supercritical flow enters upstream of a pre-existing current," Research Data Unipd. <https://researchdata.cab.unipd.it/id/eprint/1108>